Neuron, Volume *92*

Supplemental Information

The Impact of Structural Heterogeneity on Excitation-Inhibition Balance in Cortical Networks

Itamar D. Landau, Robert Egger, Vincent J. Dercksen, Marcel Oberlaender, and Haim Sompolinsky

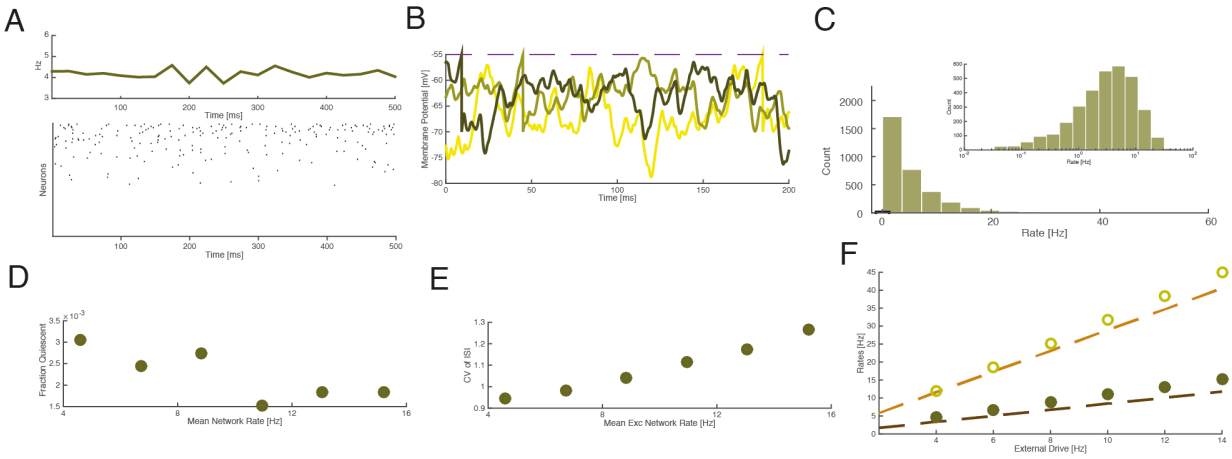

Figure S1. Related to Figure 5: Synapses Normalized by Post-Synaptic In-Degree. (A) Mean population rate and raster plot of the resulting dynamics. Neurons fire irregularly. (B) Sample voltage traces show significant temporal fluctuations near threshold. (C) Rate distribution is reasonably skewed. Inset: Log histogram of rates is roughly Gaussian. (D) Fraction of neurons silent is near zero. (E) CV_{ISI} is near 1. (F) Mean network rates follow linear balanced equations. Homeostatic plasticity that effectively normalizes synaptic strength according to postsynaptic in-degree is capable of returning the heterogeneous network to the balanced state.

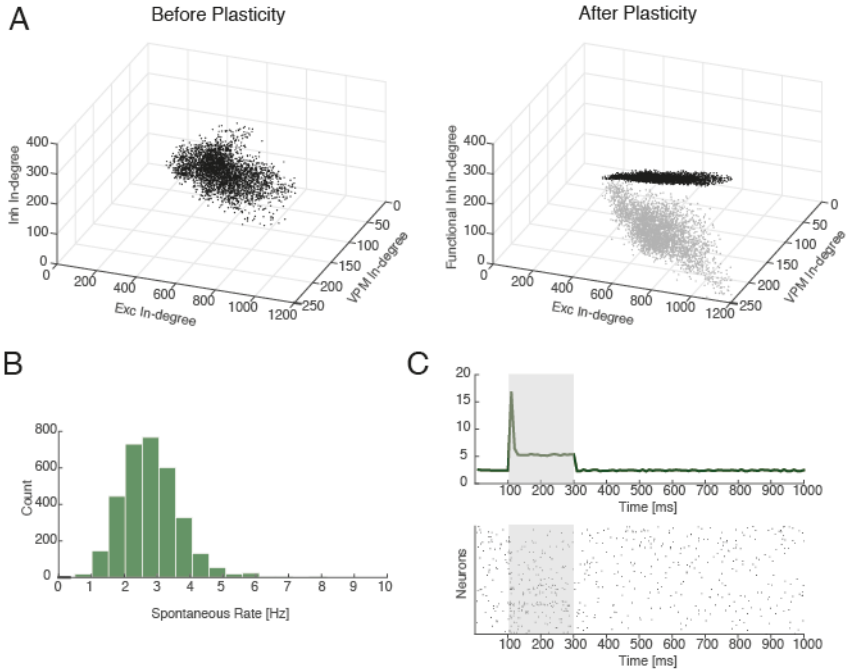

Figure S2. Related to Figure 3 and Figure 6: Homeostatic Inhibitory Plasticity on Anatomically Constrained Network, and Realistic Spontaneous and Stimulus-evoked States

(A) 3D scatter plots of functional in-degrees. Left: Before plasticity. Right: After plasticity. Despite the correlations in the anatomically constrained network, the structural in-degrees are full-rank and therefore prevent balance (see below). After plasticity, the inhibitory functional in-degrees have been aligned such that the functional in-degrees are coplanar. Grey dots: Exc and VPM functional in-degrees which are unchanged throughout plasticity. **(B-C)** Realistic spontaneous and stimulus-evoked states after plasticity. **(B)** Spontaneous State: We drive the network with constant firing VPM neurons such that the mean rate of the excitatory population is near 2.5 Hz for 60 s. Nearly all neurons fire and no excitatory neurons fire above 10 Hz (compare Fig 6E-middle, before plasticity). **(C)** Stimulus-evoked State: we simulate a ramp-and-hold stimulus with an initial volley of VPM activity followed by continued moderate rates through the end of the 200 ms stimulus period. The average percentage of unresponsive neurons on single trials was 49% (compared to 78% before plasticity), and 0% were unresponsive throughout all 100 trials (compared to 49% before plasticity). (Compare Fig 6D-middle, without plasticity and Fig 6C for fraction unresponsive)

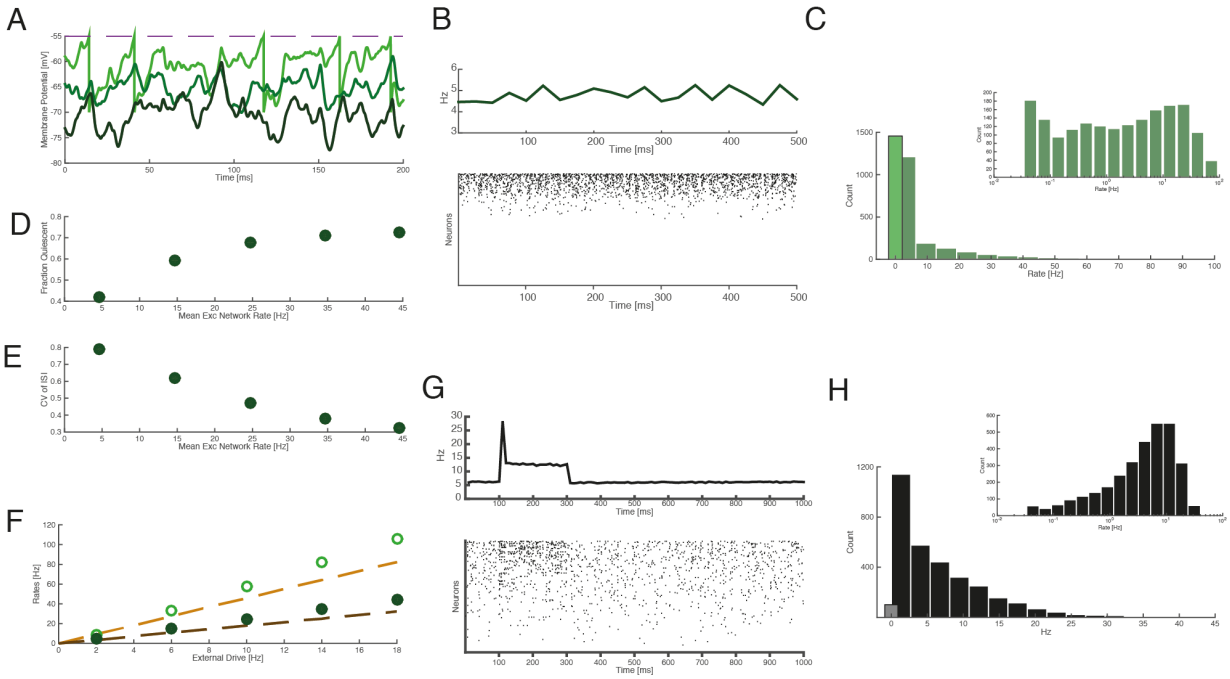

Figure S3. Related to Figure 5 and Figure 6: Alternative Connectivity Matrix from Anatomy.
An additional connectivity matrix was generated under alternative assumptions regarding the relationship between the probability of connectivity between different types and the geometric overlap. As described in Supplemental Experimental Procedures, in the original anatomically constrained matrix Exc-to-Exc synapses were assigned according to overlap with dendritic length while connections between other pairs of cell-types were assigned according to dendritic surface area. In the alternative matrix all synapses are assigned according to dendritic surface area, yielding higher correlations of input connectivity from different types and therefore less dynamic imbalance. **(A)** Sample voltage traces of three typical neurons. The membrane potentials are somewhat separated yet also fluctuate significantly. **(B)** Mean population rate and raster plot. A large fraction of neurons are silent. **(C)** Rate distribution with totally silent marked by bar with black edge. The distribution is extremely skewed, as in the original anatomically constrained network. **(D)** Fraction silent over 60s of simulation vs network rate. The fraction of neurons totally silent is less than in the anatomically constrained network but still unrealistically high. **(E)** CV_{ISI} as a function of network rate. The CV_{ISI} is low and drops with increasing firing rate, similar to that of the anatomically constrained network. **(F)** Mean population rates vs external drive. The rates deviate from the balance theory predictions, but less than in the original anatomically constrained matrix. **(G)** PSTH and rasterplot of the alternative matrix with adaptation. The strength of adaptation necessary to recover balance is approximately equal that found in the literature. The percentage of neurons unresponsive to stimulus is below 6% **(H)** Spontaneous rate distribution. The percentage of neurons silent is 3%.

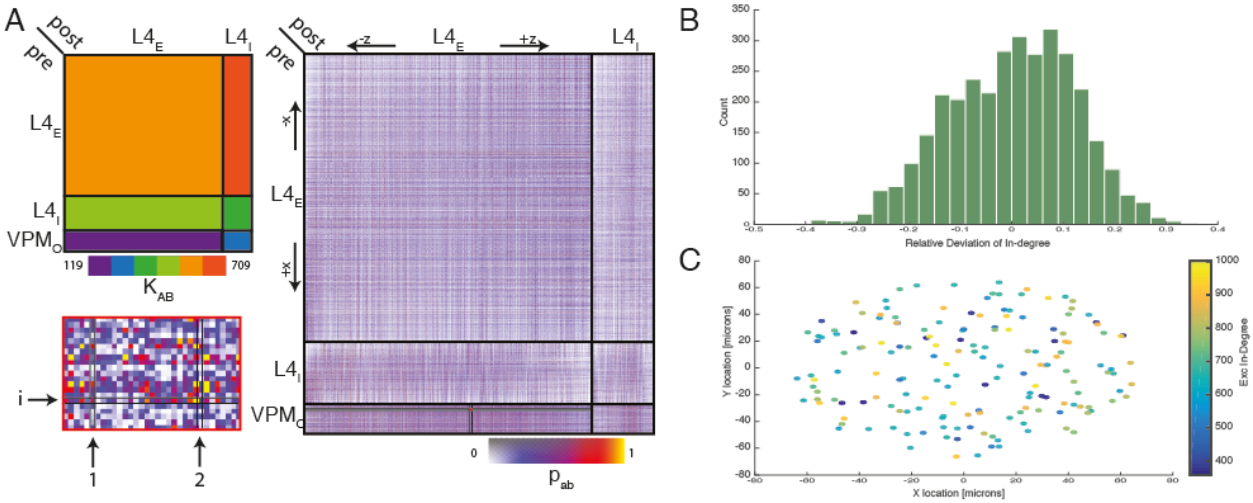

Figure S4. Related to Figure 5: Anatomical Sources of Heterogeneity. Analysis of the anatomically constrained network. **(A)** Top Left: Cell-type-to-cell-type matrix of mean total number of connections. Right: Cell-to-cell matrix of connection probabilities. Presynatpic neurons are ordered according to cell-type and then horizontal location within the barrel. Postsynaptic neurons are ordered according to cell-type and then vertical location within L4. Spatial trends are apparent, for example, from the edges of the barrel to barrel-center. Bottom Left: Zoomed-in sample of the connectivity matrix shows local heterogeneity. **(B)** Heterogeneity is independent of dendritic length. We subtract from each neuron's in-degree the mean in-degree of cells with similar dendritic length, and then divide by the overall mean in-degree. The resulting histogram has significant standard deviation, i.e. even after correcting for dendritic length the width of the in-degree distribution is a substantial fraction of the mean (0.12). **(C)** Heterogenetiy is independent of location. A scatterplot of all excitatory neurons at the subregion in the very center of the barrel. Color represents excitatory in-degree. Neighboring neurons differ significantly in their in-degree. We divide the region into 42 subregions and find that the average CV_K within each bin is 0.22.

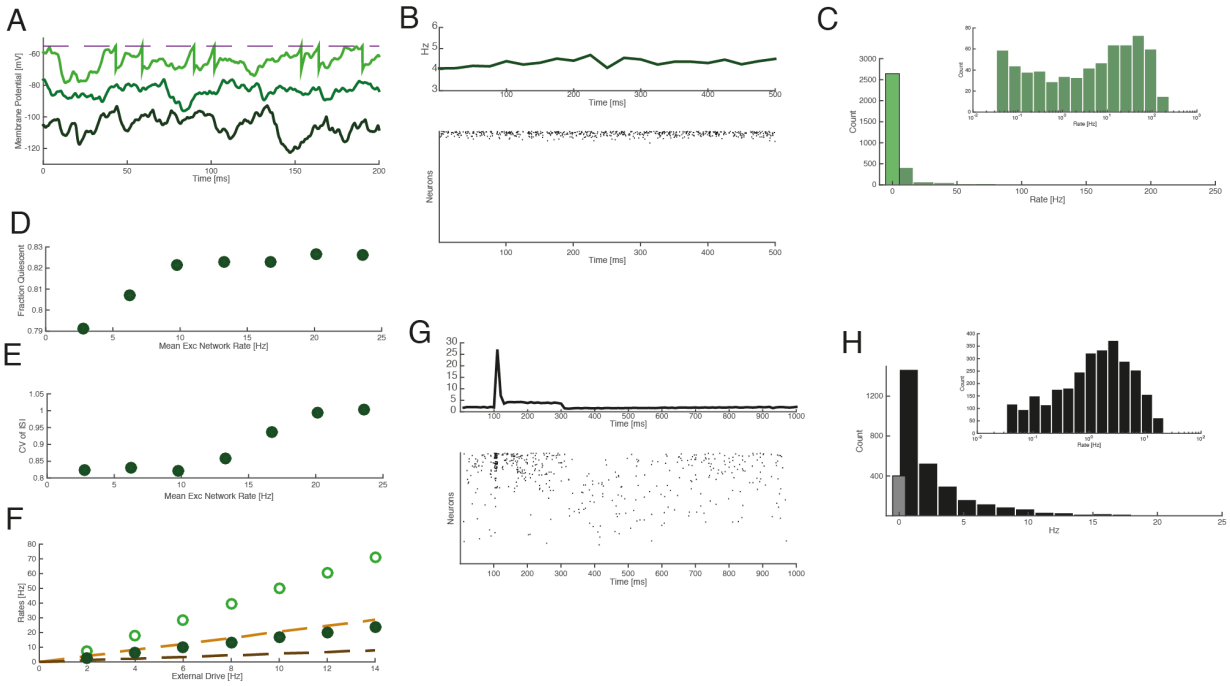

Figure S5. Related to Figure 5 and Figure 6: Analog Synaptic Strengths. Beyond probability of connection between each pair of neurons, the connectivity model provides an estimated number of contacts between each pair. Assuming a linear relationship between number of contacts and synaptic strength we build an analog connectivity matrix. The distribution of synaptic weights that arises is long-tailed (mean Exc-to-Exc EPSP = 0.42 mV, std = 0.20 mV, max = 3.7 mV). Note that in this network input connectivity is correlated with incoming synaptic strength – neurons with more inputs are likely to have stronger inputs. **(A)** Sample voltage traces of three typical neurons. Note the scale of the y-axis – the membrane potentials are very broadly distributed, and their fluctuations are large. **(B)** Mean population rate and raster plot. A large majority of neurons are silent. **(C)** Rate distribution with totally silent marked by bar with black edge. The distribution is extremely skewed as in the original anatomically constrained matrix. **(D)** Fraction silent over 60s of simulation vs network rate. **(E)** CV_{ISI} as a function of network rate. In contrast to the network with binary synapses, the CV_{ISI} is high and grows with increasing network rate. **(F)** The mean rates diverge significantly from the linear balanced predictions. **(G-H)** This network requires stronger adaptation to recover balance. We use an adaptation current that is 2.5 times stronger in amplitude than that used for the binary network. **(G)** PSTH and rasterplot of the analog connectivity matrix with adaptation. Stimulus response recovers realistic firing properties. Less than 20% of neurons remain unresponsive to stimulus. **(H)** Spontaneous rate distribution with adaptation. Inset: Log histogram. Adaptation returns the analog network to a balanced state with realistic rate distribution. The connectivity matrix with long-tailed synaptic weights as well as heterogeneous input connectivity exhibits loss of balance similar to the binary matrix except that fluctuations continue to contribute to dynamics. Adaptation recovers balance but must be somewhat stronger than in the binary setting.

$\bar{K}^{EE}$	**L2/3**	**L4**	**L5**	**L6**
L2/3	1119	884	506	56
L4	457	881	284	91
L5	713	722	691	389
L6	204	300	405	791
CV_K^{EE}	**L2/3**	**L4**	**L5**	**L6**
L2/3	0.34	0.42	0.35	0.47
L4	0.66	0.40	0.55	0.45
L5	0.58	0.46	0.39	0.42
L6	0.36	0.39	0.33	0.23

Table S1. Related to Table 1: Substantial Heterogeneity Throughout Cortical Column

Anatomically-constrained estimates of the mean in-degrees, $\bar{K}^{EE}$ and coefficients of variation of the in-degrees, CV_K^{EE}, between all layers of the D2 column of barrel cortex. Table column represents presynaptic layer, table row represents postsynaptic layer.

SUPPLEMENTAL EXPERIMENTAL PROCEDURES

Structural Bounds on Balance. Related to Heterogeneous Balance Theory

Here we formally derive the structural bounds for a heterogeneous network to maintain balance, i.e. the limits on the extent of heterogeneity as given by the Structural Imbalance, Δ (Eqn 3 of main text).

For concreteness we study the generative model described in the Experimental Procedures. In short, we study heterogeneous networks consisting of populations, *E* and *I*, and external population *O* in which each neuron i of type A has a given set of relative in-degrees $\left(k_i^{AE}, k_i^{AI}, k_i^{AO}\right)$. The connectivity matrix from type B to type A is given by $\mathbf{C}_{ij}^{AB}$ in which each row i, $k_i^{AB}K^{AB}$ elements are chosen at random to be 1 and all the rest are 0, where K^{AB} is the population average in-degree.

For ease of notation in what follows we introduce the parameters j^{AB} which are $O(1)$ relative to threshold (units: current * time), and K, a scaling parameter that scales the mean in-degree of every type-to-type pathway. Following (van Vreeswijk & Sompolinsky 1998), we make synapses strong by scaling individual synapses by $1/\sqrt{K}$. We write the strength of a single connected synapse as $W^{AB} = \sqrt{K}\,\frac{j^{AB}}{K^{AB}}$.

The time-averaged net current onto neuron i is

$$I_i^A = \left\langle \sum_B \sum_{j=1}^{N^B} \mathbf{C}_{ij}^{AB} W^{AB} s_j^B(t) + I_i^{AO}(t) \right\rangle$$

where $s_j^B(t)$ is the neuron's normalized synaptic trace which has time-average r_j^A, the single-neuron firing rate. We assume the external drive I_i^{AO} is $O\left(\sqrt{K}\right)$ and constant, and we denote it as $I_i^{AO} = \sqrt{K} k_i^{AO} J^{AO} r^O$. We assume that r_j^A is uncorrelated with $\mathbf{C}_{ij}^{AB}$ so that

$$I_i^A = \sqrt{K}\left(\sum_B k_i^{AB} j^{AB} r^B \right)$$

Balance requires that all but a negligible fraction of neurons have average net current that is near threshold, which yields the balance conditions of Eqn 2 in the main text. Here we study the balance conditions in the large K limit, which yield $\tilde{I}_i^A \equiv \sum_B k_i^{AB} j^{AB} r^B = 0$.

Fully Correlated In-degrees

To begin with we suppose that the relative in-degrees are fully correlated such that $k_i^{AB} = k_i^A$. In this case the balance condition is

$$\tilde{I}_i^A = k_i^A \sum_B j^{AB} r^B = 0$$

which reduces quite simply to the balance condition identical to that of the homogeneous network with the same synaptic strengths and mean in-degrees, namely $\sum_B j^{AB} r_0^B = 0$. As shown in (van Vreeswijk & Sompolinsky 1998), in the balance regime where external drive is strong enough to ensure non-zero network activity and inhibition dominates in order to maintain stability ($j^{EO}/j^{IO} > j^{EI}/j^{II} > j^{EE}/j^{IE}$) there exists a unique balance solution r_0^A such that $\sum_B j^{AB} r_0^B = 0$. Such a network will reach an asynchronous steady-state with mean population firing rates given by r_0^A.

Deviation From Fully Correlated

We now allow for deviations from fully correlated in-degrees and derive a bound on the extent of such deviations that will still enable a balance solution.
We decompose the relative in-degrees into correlated component, given by the average across pre-synaptic populations, $k_i^A = \frac{1}{3}\sum_B k_i^{AB}$, and deviations, δk_i^{AB}. We write for each relative in-degree:

$$k_i^{AB} = k_i^A + \delta k_i^{AB}.$$

In order for $\tilde{I}_i^A \sim \frac{1}{\sqrt{K}}$ for all but a negligible fraction of neurons we require that $\mathbf{E}\left[\tilde{I}_i^A\right] \sim \frac{1}{\sqrt{K}}$ and $\mathrm{Var}\left[\tilde{I}_i^A\right] \sim \frac{1}{K}$.
For the condition on the mean we have

$$\mathbf{E}\left[\tilde{I}_i^A\right] = \sum_B j^{AB} r^B \sim \frac{1}{\sqrt{K}}$$

so that the mean population rates must be identical to the fully correlated case, r_0^A, up to a correction of $O\left(1/\sqrt{K}\right)$.
With those mean rates we have for individual neurons:

$$\tilde{I}_i^A = \sum_B \delta k_i^{AB} j^{AB} r_0^B + O\left(\frac{1}{\sqrt{K}}\right)$$

From here the condition on the variance leads us to the structural bound on maintaining balance:

$$\Delta \sim \frac{1}{K}$$

where $\Delta \equiv \mathbf{E}\left[\left(\delta k_i^{AB}\right)^2\right]$, is the "structural imbalance" as in Eqn 3 of the main text, which guarantees that

$$\mathrm{Var}\left[\tilde{I}_i^A\right] \sim \frac{1}{K}$$

Recovering Balance by Homeostatic Inhibitory Plasticity. Related to Homeostatic Plasticity Rules

We now assume a heterogeneous network with significant structural imbalance and therefore no balanced state solution, and we proceed to study solutions via homeostatic plasticity of inhibitory synapses in which changes to synapse strength depend only on postsynaptic firing. We write the synaptic strength from inhibitory neuron j onto neuron i of type A as

$$W_{ij}^{AI} = W^{AI}\left(1+\delta J_i^{AI}\right)$$

where W^{AI} is the initial strength of inhibitory synapses (which is negative) as above. Then the net inhibitory synaptic input is

$$\sum_{j=1}^{N^I} \mathbf{C}_{ij}^{AI} W_{ij}^{AI} r_j^I = \sqrt{K} k_i^{AI,struct} j^{AI}\left(1+\delta J_i^{AI}\right) r^I$$

where $k_i^{AI,struct}$ are the structural in-degrees. Therefore the balance conditions in the large K limit are:

$$k_i^{AI,struct} j^{AI}\left(1+\delta J_i^{AI}\right) r^I + k_i^{AE} j^{AE} r^E + k_i^{AO} j^{AO} r^O = 0$$

In order to find the necessary synaptic changes that will enable balance we simply solve for δJ_i^{AI}:

$$\delta J_i^{AI} = \frac{1}{k_i^{AI,struct}\left|j^{AI}\right| r^I}\left(k_i^{\mathrm{AI},struct} j^{AI} r^I + k_i^{AE} j^{AE} r^E + k_i^{AO} j^{AO} r^O\right)$$

The mean firing rates r^E and r^I must be positive but are otherwise unconstrained so that we find a set of solutions parameterized by two positive parameters which we write in the form of $\alpha^E = r^E/r^I$ and $\alpha^O = r^O/r^I$. For a fixed set of structural in-degrees and any choice of positive α^E and α^I, balance can be achieved by inhibitory synaptic changes given by:

$$\delta J_i^{AI} = \frac{1}{k_i^{AI,str}\left|j^{AI}\right|}\left(k_i^{AI,str} j^{AI} + k_i^{AE} j^{AE}\alpha^E + k_i^{AO} j^{AO}\alpha^O\right) \qquad (2)$$

The parameters α^E and α^I determine the ratios between mean population firing rates at steady state which will emerge dynamically in order to achieve balance.

To better understand this set of synaptic solutions we examine the resulting "functional in-degrees", $k_i^{AI} = k_i^{AI,struct}\left(1+\delta J_i^{AI}\right)$. From SI Eqn 2, (or directly from SI Eqn 1 above) we find that in order to enable balance the inhibitory functional in-degrees must satisfy the following equation (Eqn 4 of main text):

$$k_i^{AI} = \frac{1}{\left|j^{AI}\right|}\left(k_i^{AE} j^{AE}\alpha^E + k_i^{AO} j^{AO}\alpha^O\right)$$

This requirement can be understood geometrically as meaning that the N triples defining each neuron's in-degrees, $\left(k_i^{AE}, k_i^{AI}, k_i^{AO}\right)$ must be coplanar (see Fig 3). Note that these are two distinct planes, one for each post-synaptic population, and that the mean population rates r^E and r^I are determined by the relative orientations between these two planes. We note also that the fully correlated case where $k_i^{AB} = k_i^A$ is a special case in which the in-degrees are colinear.

Functional Imbalance Measure

In order to construct a measure for Functional Imbalance during plasticity, we define two 3x3 matrices

$$\left[M^A\right]_{B,C} = \mathbf{E}\left[k_i^{AB}k_i^{AC}\right]j^{AB}j^{AC}$$

and observe that $\mathbf{r}^T\mathbf{M}^A\mathbf{r} = \mathbf{E}\left[\left(\tilde{I}_i^A\right)^2\right]$ where $\mathbf{r}$ is the 3D column vector of population firing rates. The balance requirement is that $\mathbf{E}\left[\left(\tilde{I}_i^A\right)^2\right] \sim \frac{1}{K}$ for both populations, which in the large K limit requires that $\mathbf{r}$ is an eigenvector of both matrices $\mathbf{M}^A$ with zero eigenvalue. Given functional in-degrees $\left\{k_i^{AB}\right\}$ we are interested in the minimum over possible firing rate vectors $\mathbf{r}$, and so we define as "functional imbalance":

$$E\left(\left\{k_i^{AB}\right\}\right) = \min_{\mathbf{r}:\|\mathbf{r}\|=1,\, r^B>0} \sqrt{\frac{1}{2}\sum_A \mathbf{r}^T\mathbf{M}^A\mathbf{r}}$$

and plot this measure throughout the plasticity in Fig 3. Balance is attained when $E \sim 1/\sqrt{K}$.

Plasticity Rule and Fixed Point Equations

We model a homeostatic plasticity rule on inhibitory synapses as an additive synaptic scaling in which individual synapse strength of connected neurons ($C_{ij}^{AI} = 1$) depends on a low-pass filtered version of the post-synaptic neuron's firing rate

$$\frac{\mathrm{d}W_{ij}^{AI}}{\mathrm{dt}} = -\frac{1}{\tau_w}W_{ij}^{AI} + \eta^A z_i^A(t)$$

where z_i^A is obtained by low-pass filtering neuron i's spike train:

$$\frac{\mathrm{d}}{\mathrm{dt}}z_i^A = -\frac{1}{\tau_l}z_i^A + \sum_k \delta\left(t - t_{i,k}^A\right)$$

where $t_{i,k}^A$ is the time of the k th action potential of neuron i of type A.

At steady-state, $z_i^A \approx \tau_l r_i^A$ so that writing $\lambda^A = \tau_w\eta^A\tau_l$ the fixed point equation for the synaptic strengths are:

$$W_{ij}^{AI^*} = \lambda^A r_i^{A^*}$$

A quiescent neuron will therefore have zero inhibition, which is a contradiction since all neurons receive non-zero excitation. Therefore all neurons will be active.

λ^A is chosen so that $\lambda^A r^O \sim 1$. Thus a neuron that fires at a high firing rate ($r_i^{A^*}/r^O \sim \sqrt{K}$) will have inhibition that is an order of magnitude larger than its excitation, which is a contradiction. Therefore all neurons will have $O(1)$ firing rates.

For a neuron to have $O(1)$ firing rate its functional in-degree ($k_i^{AI} = k_i^{AI,str}W_{ij}^{AI}$) must satisfy the local balance equation. This yields

$$r_i^{A^*} = \frac{1}{\lambda^A}\frac{k_i^{AE}j^{AE}r^{E^*} + k_i^{AO}j^{AO}r^O}{k_i^{AI,str}\left|j^{AI}\right|r^{I^*}}$$

We can take the population average to arrive at equations for the population mean rates:

$$r^{A^*} = \frac{1}{\lambda^A}\left(\mathbf{E}\left[\frac{k_i^{AE}}{k_i^{AI,str}}\right]\frac{j^{AE}r^E}{\left|j^{AI}\right|r^I} + \mathbf{E}\left[\frac{k_i^{AO}}{k_i^{AI,str}}\right]\frac{j^{AO}r^O}{\left|j^{AI}\right|r^I}\right)$$

Writing $\gamma^{AB} \equiv \mathbf{E}\left[k_i^{AB}/k_i^{AI,str}\right]$ this yields two quadratic equations for the two unkowns:

$$\lambda^A\left|j^{AI}\right|r^{I^*}r^{A^*} = \gamma^{AE}j^{AE}r^{E^*} + \gamma^{AO}j^{AO}r^O$$

The equation for $A = I$ yields the steady-state inhibitory rate:

$$r^{I^*} = \sqrt{\frac{\gamma^{IE} j^{IE} r^{E^*} + \gamma^{IO} j^{IO} r^{O}}{\lambda^{I} \left| j^{II} \right|}}$$

And after substitution and rearranging this yields a cubic equation for the excitatory rate:

$$\frac{\left(\lambda^{E} j^{EI}\right)^2 \gamma^{IE} j^{IE}}{\lambda^{I} \left| j^{II} \right|} \left(r^{E^*}\right)^3 + \left(\frac{\left(\lambda^{E} j^{EI}\right)^2 \gamma^{IO} j^{IO} r^{O}}{\lambda^{I} \left| j^{II} \right|} - \left(\gamma^{EE} j^{EE}\right)^2 \right) \left(r^{E^*}\right) - 2\gamma^{EE} \gamma^{EO} j^{EE} j^{EO} r^{O} r^{E^*} - \left(\gamma^{EO} j^{EO} r^{O}\right)^2 = 0$$

This is a cubic equation with real coefficients and negative constant term so it must have at least one positive real root, therefore a balanced fixed-point solution exists.

Self-consistency of Adaptation-Facilitated Balance and the Requirements for All Neurons To Be Active. Related to Adaptation Dynamics and Theory

Following the notation introduced in the Experimental Procedures, the dynamics of the adaptation current for a given neuron are given by:

$$K\tilde{\tau}_{ad}^{A}\frac{dI_{ad}^{A}}{dt}=-I_{ad}^{A}+\sqrt{K}\,j_{ad}^{A}\tilde{\tau}_{ad}^{A}\sum_{\{t_{sp}\}}\delta\left(t-t_{sp}\right)$$

Where $\{t_{sp}\}$ are all past spike times of the given neuron, and both $\tilde{\tau}_{ad}^{A}$ and j_{ad}^{A} are $O(1)$. Thus the steady-state mean adaptation current for a neuron firing at rate r_i^A is $\sqrt{K}\,j_{ad}^{A}\tilde{\tau}_{ad}^{A}r_i^A$, which enters the leading term of the net current:

$$I_i^A=\sqrt{K}\left(\sum_B k_i^{AB}j^{AB}r^B-j_{ad}^{A}\tilde{\tau}_{ad}^{A}r_i^A\right)$$

The balance conditions now depend locally on each neuron's own firing rate:

$$\sum_B k_i^{AB}j^{AB}r^B-j_{ad}^{A}\tilde{\tau}_{ad}^{A}r_i^A=0$$

which can be satisfied if the local firing rates satisfy the threshold-linear rate equations (Eqn. 5):

$$r_i^A=\frac{1}{j_{ad}^{A}\tilde{\tau}_{ad}^{A}}\left[\sum_B k_i^{AB}j^{AB}r^B\right]_+$$

These must be solved self-consistently together with the population rates.

We aim to derive the conditions on the adaptation current that will ensure a fully active network so we assume all but a negligible fraction of neurons in the network are active, and then require self-consistency.

If all neurons are active the local rate equations are linear. Averaging over each entire population yields the two linear population rate equations (Eqn. 6):

$$\left(\sum_B j^{AB}r^B\right)-j_{ad}^{A}\tilde{\tau}_{ad}^{A}r^A=0$$

Note that in this case the population rates are independent of the shape of the in-degree distribution.
These equations have solutions

$$r^E=A^E r^O$$
$$r^I=A^I r^O$$

where

$$A^E=\frac{\left(j^{II}-j_{ad}^{I}\tilde{\tau}_{ad}^{I}\right)j^{EO}-j^{EI}j^{IO}}{j^{EI}j^{IE}-\left(j^{EE}-j_{ad}^{E}\tilde{\tau}_{ad}^{E}\right)\left(j^{II}-j_{ad}^{I}\tilde{\tau}_{ad}^{I}\right)}$$
$$A^I=\frac{\left(j^{EE}-j_{ad}^{E}\tilde{\tau}_{ad}^{E}\right)j^{IO}-j^{IE}j^{EO}}{j^{EI}j^{IE}-\left(j^{EE}-j_{ad}^{E}\tilde{\tau}_{ad}^{E}\right)\left(j^{II}-j_{ad}^{I}\tilde{\tau}_{ad}^{I}\right)}$$

Following (van Vreeswijk & Sompolinsky 1998) directly, the following set of constraints on system parameters necessary in order to achieve balance:

$$\frac{j^{EO}}{j^{IO}}>\frac{j^{EI}}{j^{II}-j_{ad}^{I}\tilde{\tau}_{ad}^{I}}>\frac{j^{EE}-j_{ad}^{E}\tilde{\tau}_{ad}^{E}}{j^{IE}}$$

Note that this places a limit on the strength of inhibitory adaptation.

We can now reinsert the population rates into the local rate equations to ensure self-consistency, i.e. to ensure that all but a negligible fraction of neurons are active. This requires that the net synaptic input be positive:

$$\sum_B k_i^{AB} j^{AB} r^B = \left(k_i^{AE} j^{AE} A^E + k_i^{AI} j^{AI} A^I + k_i^{AO} j^{AO} \right) r^O > 0$$

Therefore the final condition for a fully active network, which is independent of external drive, is the following set of inequalities:

$$k_i^{AE} j^{AE} A^E + k_i^{AI} j^{AI} A^I + k_i^{AO} j^{AO} > 0$$

for all but a negligible fraction of neurons.

Details of Anatomically Constrained Connectivity Model

The initial stage of constructing the anatomically constrained connectivity model ('dense statistical connectome') is reconstructing anatomical landmarks (i.e., the outlines of the L4 barrels representing the 24 large facial whiskers, the pial and white matter surfaces) in vS1 in order to generate a standardized 3D geometric reference frame with a resolution of 50 μm (Egger et al. 2012). Second, the number and 3D distribution of all excitatory and inhibitory neuron somata in rat vS1 and VPM are measured with respect to the anatomical landmarks (Meyer et al. 2013), and then registered to the reference frame model of rat vS1 at a resolution of $50\mu m^3$. This is achieved by double imunolabeling for NeuN (neuron-specific nuclear protein), which marks all neurons, and GAD67 (67 kDa isoform of glutamate decarboxylase), which marks only inhibitory neurons. The entire barrel cortex is then imaged with high-resolution, large-scale confocal microscopy in 50 or 100 μm slices and cells counted by automatic processing (Meyer, Wimmer, Oberlaender, et al. 2010; Oberlaender et al. 2009). This yields an excitatory and inhibitory somata density map in real three-dimensional space for each of the 24 columns of the barrel cortex (Meyer et al. 2013).

The next stage is to identify subtypes of cells and generate a library of axonal/dendritic morphologies for each cell type. VPM axons (Oberlaender et al., Cereb Cortex 2012) and dendrites/axons in vS1 were reconstructed from *in vivo*-labeled excitatory neurons (Narayanan et al., 2015); inhibitory morphologies were reconstructed from *in vitro*-labeled cells, provided by Dirk Feldmeyer (see Koelbl et al.) and Bert Sakm. Neurons are biocytin-labeled *in vivo*, enabling the tracing of full axon/dendrite morphologies. Then 50 or 100 μm slices are scanned by brightfield microscopy and the full image is reconstructed. Boutons are marked manually from high-resolution images of a subset of axons, in order to yield bouton density per length of axon. As 1st-order approximation, spine density per dendrite length is taken as constant over all cell-types. Automated clustering of morphological features has yielded nine distinct excitatory cell-types, each with a particular laminar distribution (Oberlaender et al. 2012; Narayanan et al. 2015). Inhibitory neurons are stained in slice so that their axons are dendrites are often clipped. The clipped morphologies are used to estimate morphological statistics of inhibitory cells, which are then used to construct full *in vivo*-sized sample morphologies.

Network upscaling begins by assigning a cell-type to each soma location, based on the local relative density of each cell type. Next each soma is assigned a dendritic and axonal morphology of the appropriate cell type. This process of "repopulating" the barrel cortex with full morphological neurons, combined with spine density estimates, then yields cell-specific spine density maps.

The connectivity estimate is generated based on the assumption that at a resolution of 50 μm, dendritic-axonal overlap is a good predictor of the location of synaptic contacts to particular post-synaptic partners (Meyer, Wimmer, Hemberger, et al. 2010; Lang et al. 2011).

Each cell receives synaptic contacts within a given 50^3 μm^3 voxel in accordance with the extent to which its dendrite projects into this voxel relative to the rest of the population's dendrites. For each type of incoming synapse of type $B \in \{E, I\}$, each neuron i of type A is given a spatial "post-synaptic target density", $s_i^{AB}(\mathbf{x})$. Excitatory synapses onto excitatory cells tend to be formed on dendritic spines, while inhibitory synapses and excitatory synapses onto inhibitory cells are formed anywhere on the dendritic shaft. We therefore differentiate between Exc-to-Exc synapses and all others. Since dendritic spines have been reported to be spatially distributed proportionally to dendritic length, $s_i^{EE}(\mathbf{x})$ is assigned proportional to dendritic length in voxel $\mathbf{x}$, while for the three other synapse types $s_i^{AB}(\mathbf{x})$ is proportional to dendritic area. We also construct an alternative connectivity matrix in which contacts between all pairs of types are assigned proportional to dendritic surface area. The results of simulations on this network are presented in SI Fig 1.
The total post-synaptic target density for incoming synapses of type B in voxel $\mathbf{x}$ is $S^B(\mathbf{x}) = \sum_A \sum_i s_i^{AB}(\mathbf{x})$.

Then the probability, $p_i^{AB}(\mathbf{x})$ that neuron i of type A is contacted by any incoming bouton of type B in voxel $\mathbf{x}$ is simply the ratio:

$$p_i^{AB}(\mathbf{x}) = \frac{s_i^{AB}(\mathbf{x})}{S^B(\mathbf{x})}$$

Then given a number of incoming boutons b of type B in voxel $\mathbf{x}$, the number of these which synapse with neuron i of type A is distributed Binomial$\left(p_i^{AB}(\mathbf{x}),b\right)$.

Each neuron has a spatial bouton density, $b_j^B(\mathbf{x})$ which is proportional to axonal length within each voxel. Given the small values of $p_i^{AB}(\mathbf{x})$, the distribution of the number of the number of synapses from neuron j of type B onto neuron i of type A in voxel $\mathbf{x}$ is reasonably approximated by a Poisson distribution with mean

$$I_{ij}^{AB}(\mathbf{x}) = b_j^B(\mathbf{x}) \cdot \frac{s_i^{AB}(\mathbf{x})}{S^B(\mathbf{x})}$$

This yields a subcellular distribution of synaptic contacts, which for our purposes we reduce to the single neuron level by computing the net expected number of contacts from neuron j to neuron i across all voxels:

$$\mathbf{I}_{ij}^{AB} = \sum_{\mathbf{x}} I_{ij}^{AB}(\mathbf{x}) = \sum_{\mathbf{x}} b_j^B(\mathbf{x}) \cdot \frac{s_i^{AB}(\mathbf{x})}{S^B(\mathbf{x})}$$

Finally we derive the anatomically constrained connectivity matrix as the probability of a non-zero number of contacts from neuron j to neuron i: $\mathbf{P}_{ij}^{AB} = 1 - \exp(-\mathbf{I}_{ij}^{AB})$.